

MeV-scale reheating temperature and cosmological production of light sterile neutrinos

Takuya Hasegawa,^{1,2} Nagisa Hiroshima,^{2,3,4} Kazunori Kohri,^{1,2,5}

Rasmus S. L. Hansen,^{6,7,8} Thomas Tram,^{7,9} and Steen Hannestad⁷

¹*The Graduate University of Advanced Studies (Sokendai), Tsukuba 305-0801, Japan*

²*Theory Center, IPNS, KEK, Tsukuba 305-0801, Japan*

³*RIKEN Interdisciplinary Theoretical and Mathematical Sciences (iTHEMS), Wako, Saitama 351-0198, Japan*

⁴*Department of Physics, University of Toyama, 3190 Gofuku, Toyama 930-8555, Japan*

⁵*Kavli IPMU (WPI), UTIAS, The University of Tokyo, Kashiwa, Chiba 277-8583, Japan*

⁶*Max-Planck-Institut für Kernphysik, Saupfercheckweg 1, 69117 Heidelberg, Germany*

⁷*Department of Physics and Astronomy, University of Aarhus, Ny Munkegade 120, DK8000 Aarhus C, Denmark*

⁸*Niels Bohr International Academy and DARK, Niels Bohr Institute, Blegdamsvej 17, 2100 Copenhagen, Denmark*

⁹*Aarhus Institute of Advanced Studies (AIAS), Aarhus University, DK8000 Aarhus C, Denmark*

(Dated: August 10, 2020)

We investigate how sterile neutrinos with a range of masses influence cosmology in MeV-scale reheating temperature scenarios. By computing the production of sterile neutrinos through the combination of mixing and scattering in the early Universe, we find that light sterile neutrinos, with masses and mixings as inferred from short-baseline neutrino oscillation experiments, are consistent with big-bang nucleosynthesis (BBN) and cosmic microwave background (CMB) radiation for the reheating temperature of $\mathcal{O}(1)$ MeV if the parent particle responsible for reheating decays into electromagnetic components (radiative decay). In contrast, if the parent particle mainly decays into hadrons (hadronic decay), the bound from BBN becomes more stringent. In this case, the existence of the light sterile neutrinos can be cosmologically excluded, depending on the mass and the hadronic branching ratio of the parent particle.

I. INTRODUCTION

The anomaly in short-baseline (SBL) neutrino experiments is a long-standing problem in the neutrino sector. Since the LSND collaboration reported a $3.8\text{-}\sigma$ anomaly in their results in the 1990s [1], various experimental projects have been performed to investigate the origin. The Mini-BooNE collaboration found the similar anomaly in both the neutrino and anti-neutrino modes [2], and it remains after the update in the experiment [3]. In addition to the accelerator neutrino oscillation experiments, similar anomalies have been found in other types of experiments, *e.g.* reactor neutrino experiments such as Daya Bay [4] and Double Chooz [5], or Gallium experiments such as SAGE [6–8] and GALLEX [9–11].

The existence of the eV-scale sterile neutrino produced through the mixing with active neutrinos is a well-motivated scenario to explain the anomaly. This scenario has been tested in different kinds of experiments. In contrast to the appearance experiments, disappearance experiments such as MINOS/MINOS+ [12] and NO ν A [13] reported the results disfavoring the existence of such a sterile neutrino. The IceCube collaboration also investigated a signature of the conversion from active to sterile neutrinos in the atmospheric neutrino spectrum and gave a strong constraint on the parameter space of the light sterile neutrino for the SBL neutrino anomaly [14]. The origin of the anomaly is still under debate, and future experimental programs such as the SBN experiment [15] and the JSNS² experiment [16] are expected to unveil the origin.

Cosmological observations are another important probe of sterile neutrinos. If such light sterile neutrinos exist and have an appreciable mixing with active neutrinos, they are abundantly produced in the early Universe and affect the big-bang nucleosynthesis (BBN) and the cosmic microwave background (CMB) radiation. In Refs. [17–20], it was shown that the light sterile neutrino inferred from the SBL anomaly is completely thermalized well-before the onset of BBN or the last scattering of CMB. This means the existence of the light sterile neutrino is strongly excluded from BBN and CMB. The tension could be alleviated by suppressing the thermalization of sterile neutrinos. Several scenarios have been proposed as the suppression mechanism: large chemical potentials of active neutrinos [18, 21–23], self-interaction or non-standard interaction of sterile neutrinos [24–29], or low reheating temperature of the Universe [30–35].

In this paper, we focus on the thermalization of sterile neutrinos in the Universe with an MeV-scale reheating temperature to solve the tension between the light sterile neutrino and cosmology. Since the sterile neutrino production through the weak interaction of active neutrinos effectively finishes when the cosmic temperature becomes $\sim \mathcal{O}(1)$ MeV, the MeV-scale reheating temperature

leads to the incomplete thermalization of sterile neutrinos, which offers the solution to the problem.

The reheating temperature of the Universe is much lower than that of the standard cosmology if there exists a long-lived massive particle and it causes reheating of the Universe. The existence of such particles is naturally expected in varieties of extensions of the standard model of particle physics. For example, curvaton, gravitino, flaton, modulus, or dilaton are well-motivated candidates for this particle. If such a long-lived particle dominates the energy density in the early epoch, the Universe experiences the early matter-dominated era before the ordinary radiation-dominated epoch, which modifies the initial condition of the standard cosmology.

This solution to the tension has been proposed in Ref. [30], and Refs. [32–34] later revisited the same scenario. In order to probe this scenario, it is necessary to simultaneously solve reheating of the Universe and the thermalization of neutrinos to accurately compute the abundance of sterile neutrinos. This is because most of the active and sterile neutrinos are produced during reheating, and matter effects on the thermalization of sterile neutrinos, cannot be neglected. However, such a computation is technically difficult, and Refs. [30, 32–34] assumed a simplified picture where sterile neutrinos are produced via vacuum oscillations after the completion of reheating. Also, the reheating temperature is fixed to be 5 MeV by hand in the studies. If sterile neutrinos are completely absent from the thermal bath, the lower bound on the reheating temperature is known to be almost 5 MeV [36, 37], but this is not true if sterile neutrinos exist, and it contributes to the energy density of the Universe. Therefore, we should not fix the reheating temperature to the typical value in advance.

Ref. [34] later updated the sterile neutrino production in the MeV-scale reheating scenario by calculating the semi-classical Boltzmann equation with effective collision terms, which include the matter effects, and provided a more detailed analysis of the thermalization of sterile neutrinos. It is however necessary to calculate the original quantum kinetic equation (QKE) instead of the semi-classical Boltzmann equation, to correctly follow the sterile neutrino thermalization unless the off-diagonal components of the collision term for neutrinos (*i.e.* the collisional damping term) dominate those of the neutrino Hamiltonian [38, 39].

The purpose of this study is to revisit the sterile neutrino thermalization in the cosmological model with an MeV-scale reheating temperature and refine the cosmological constraint on sterile neutrinos obtained in the previous studies [30, 32, 33] by performing a detailed computation of QKE and BBN. The main focus of this study is the eV-scale sterile neutrinos, motivated by the SBL neutrino anomaly.

The structure of this paper is as follows. In Sec. II we introduce our formulation for calculating

the production of active and sterile neutrinos during reheating. In Secs. III and IV we show our numerical results of the neutrino thermalization and BBN, respectively. In Sec. V we summarize the constraint on sterile neutrinos obtained from cosmological observations and ground-based experiments. Sec. VI is devoted to the conclusion.

II. STERILE NEUTRINO PRODUCTION DURING REHEATING

In this section, we explain the dynamics of cosmological models with late-time entropy production, which results in the MeV-scale reheating temperature. Also, we introduce key equations for calculating the production of sterile neutrinos during reheating.

We assume that a long-lived massive particle ϕ is responsible for reheating. In this case, the decay of ϕ induces the late-time entropy production and the subsequent dramatic particle production of the standard-model particles. Photons and charged leptons are rapidly thermalized through the electromagnetic interaction during reheating, while active neutrinos are slowly produced through the weak interaction. If the reheating temperature of the Universe is lower than the QCD scale ~ 100 MeV and the radiation-dominated epoch therefore realizes after the hadronization, active neutrinos are solely produced in the annihilation process of charged leptons $l + \bar{l} \rightarrow \nu_\alpha + \bar{\nu}_\alpha$ ($\alpha = e, \mu, \tau$), where l and \bar{l} denote the charged leptons and corresponding anti-particles, respectively. Sterile neutrinos are generated from active neutrinos through the flavor mixing as reheating proceeds. Therefore, we need to consider both neutrino collisions and neutrino oscillations in the thermalization calculations of active and sterile neutrinos.¹ Ref. [40] provided an analytical expression to estimate the sterile neutrino abundance produced in the non-resonant active-sterile mixing. The production rate of sterile neutrinos has a sharp peak at temperature T_{\max} :

$$T_{\max} \sim 13 \text{ MeV} \left(\frac{m_s}{1 \text{ eV}} \right)^{1/3}, \quad (2.1)$$

where m_s is the mass of the sterile neutrino. Hence, the abundance of sterile neutrinos is strongly suppressed compared to those obtained in the standard cosmology case if the reheating temperature is lower than T_{\max} .

The states of active and sterile neutrinos are expressed in terms of a one-body-irreducible density matrix, which is expressed in an $N_f \times N_f$ Hermitian matrix, where N_f is the number of neutrino flavors to mix. In this study, we adopt the so-called 1+1 mixing scheme in which one sterile neutrino species mixes with one active species. This approximation is reasonable when the mixing of the sterile neutrino with one active species dominates the mixing with the other active species. For the current calculation, we assume sterile neutrinos to mix with electron neutrinos, and we assume that μ neutrinos (ν_μ) and τ neutrinos (ν_τ) decouple from the neutrino oscillations. Under these assumptions, the states of spectator neutrinos, namely ν_μ and ν_τ , are degenerate, and

¹ Even if a primordial component of sterile neutrinos exists before reheating, such a component is completely diluted by the entropy production associated with reheating. Also, we do not consider any other exotic interactions among the standard-model particles and sterile neutrinos. Therefore, sterile neutrinos are produced only through the active-sterile neutrino oscillation.

it is unnecessary to separately calculate dynamical equations for each. This is because the cosmic temperature is always below $\mathcal{O}(1)$ MeV after reheating for $T_{\text{RH}} \sim \mathcal{O}(1)$ MeV, and muons and τ leptons, which are heavier than the cosmic temperature, do not exist in the thermal bath of the Universe. In the following, quantities of the spectator neutrinos are multiplied by a factor of two for summing up contributions from ν_μ and ν_τ .

Since we assume the 1+1 mixing, the density matrix of neutrinos with energy E can be expressed as a 2×2 matrix:

$$\varrho_{\mathbf{p}}(t) \equiv \varrho(E, t) = \begin{pmatrix} \varrho_{\text{aa}} & \varrho_{\text{as}} \\ \varrho_{\text{as}}^* & \varrho_{\text{ss}} \end{pmatrix}. \quad (2.2)$$

The energy of active and sterile neutrinos E is replaced with their absolute momentum p , *i.e.* $E \rightarrow p \equiv |\mathbf{p}|$, where \mathbf{p} is the three-momenta of neutrinos. This is because masses of the active neutrinos are known to be sub-eV scale [41] and safely neglected in a thermal bath of $T \sim \mathcal{O}(1)$ MeV. In addition, we restrict ourselves to the mass range of sterile neutrinos below 10 keV so that they are always relativistic before their production effectively finishes at around a temperature of the neutrino decoupling $T \sim T_{\text{dec}}$.² In Eq. (2.2), the diagonal elements of the density matrix correspond to the distribution functions of active and sterile neutrinos, *i.e.* $\varrho_{\text{aa}} = f_{\text{a}}$ and $\varrho_{\text{ss}} = f_{\text{s}}$, while the off-diagonal elements correspond to a quantum coherence between them.

The time evolution of the density matrix is governed by the momentum-dependent quantum kinetic equation (QKE) in the following [43, 44]:

$$\frac{d\varrho_{\mathbf{p}}(t)}{dt} = \left(\frac{\partial}{\partial t} - H p \frac{\partial}{\partial p} \right) \varrho_{\mathbf{p}}(t) = -i [\mathcal{H}_\nu, \varrho_{\mathbf{p}}(t)] + C[\varrho_{\mathbf{p}}(t), t], \quad (2.3)$$

where $C[\varrho_{\mathbf{p}}(t), t]$ is the collision term for the active-mixed neutrinos, H is the Hubble parameter, and \mathcal{H}_ν in the commutator is the neutrino Hamiltonian.

In this study, we neglect the neutrino chemical potentials.³ Then, it is unnecessary to follow the time evolution of anti-neutrinos separately from corresponding neutrinos, and the neutrino Hamiltonian on the right-hand side of Eq. (2.3) is reduced to

$$\mathcal{H}_\nu = \frac{M^2}{2p} - \frac{8\sqrt{2}G_F p}{3} \left[\frac{\mathbf{E}_{\text{CC}}}{m_W^2} + \frac{\mathbf{E}_{\text{NC}}}{m_Z^2} \right], \quad (2.4)$$

where G_F is the Fermi coupling constant, and m_W (m_Z) is the mass of W (Z) boson. On the right-hand side of Eq. (2.4), the first term corresponds to the vacuum oscillation of neutrinos. The

² This limitation is mandatory because non-relativistic neutrinos do not oscillate into another flavor [42], and we cannot rely on the QKE for neutrinos (Eq. (2.3)) in such cases.

³ This is a reasonable assumption since its effect on the neutrino oscillation can be safely neglected for the chemical potentials of $\mathcal{O}(10^{-10})$, as is naturally attained in the standard mechanism of baryogenesis associated with the sphaleron process. For those interested in the effect of the neutrino chemical potentials on the sterile neutrino thermalization, see *e.g.* Refs. [18, 22, 23, 45, 46].

mass matrix M in the flavor basis is related to that in the mass basis \mathcal{M} as $M^2 = U\mathcal{M}^2U^\dagger$ where U is the flavor-mixing matrix. The mass matrix \mathcal{M} for the 1+1 mixing has the explicit form of

$$\mathcal{M}^2 = \begin{pmatrix} m_1^2 & 0 \\ 0 & m_2^2 \end{pmatrix}, \quad U = \begin{pmatrix} \cos \theta & -\sin \theta \\ \sin \theta & \cos \theta \end{pmatrix}, \quad (2.5)$$

where m_1 and $m_2 (> m_1)$ are the mass eigenvalues for active and sterile neutrinos, whereas θ is the active-sterile mixing angle in a vacuum. Throughout this paper, we consider the normal mass ordering for sterile neutrinos $m_2 > m_1$, which is favored in cosmological observations [47]. The flavor-mixing matrix U uniquely determines the relation between the mass and the flavor eigenstates as

$$|\nu_a\rangle = \cos \theta |\nu_1\rangle - \sin \theta |\nu_2\rangle, \quad (2.6)$$

$$|\nu_s\rangle = \sin \theta |\nu_1\rangle + \cos \theta |\nu_2\rangle, \quad (2.7)$$

where $|\nu_a\rangle$ and $|\nu_s\rangle$ are flavor eigenstates of active and sterile neutrinos, while $|\nu_1\rangle$ and $|\nu_2\rangle$ are the mass eigenstates of lighter and heavier states, respectively. The second and third terms in Eq. (2.4) correspond to the matter effects induced by the coherent scatterings of the active-mixed neutrinos with electrons $\nu_a + e^\pm \rightarrow \nu_a + e^\pm$. The matter effect modifies the relation between the mass and the flavor eigenstates. Particularly, the second (third) term arises from the charged- (neutral-) current interaction of ν_a ($= \nu_e$) with electrons, where $\mathbf{E}_{CC} \equiv \text{diag}(\rho_e, 0)$ and $\mathbf{E}_{NC} \equiv \text{diag}(\rho_{\nu_a}, 0)$ with ρ_e and ρ_{ν_a} the energy densities of electrons and the active-mixed neutrinos, respectively.⁴

The collision term of the QKE, Eq. (2.3), is written as

$$C[\varrho_{\mathbf{p}}(t), t] = \begin{pmatrix} R_{\nu_a} & -D\varrho_{as} \\ -D\varrho_{as}^* & 0 \end{pmatrix}, \quad (2.8)$$

where R_{ν_a} is the production rate of the active-mixed neutrinos, and D is the collisional-damping factor, which gives the decoherence between states of ν_a and ν_s . We take into account the production of active neutrinos from the electron-pair annihilation, the neutrino-electron scattering, and the neutrino self-interaction. These processes are summarized in Table I of Ref. [48]. For each reaction process, we analytically reduce the dimension of momentum integrals from nine to two, without imposing any simplifying assumptions in the same way as in Ref. [48].

⁴ In a thermal bath of $T \sim \mathcal{O}(1)$ MeV, abundances of muons and τ leptons are much smaller than that of electrons due to the Boltzmann suppression. Therefore, we do not consider contributions from muons or τ leptons to the scatterings.

For numerical implementations, we expand the density matrix with Pauli matrices $\boldsymbol{\sigma} = (\sigma_x, \sigma_y, \sigma_z)$ and convert the QKE into a set of scalar equations:

$$\varrho_{\mathbf{p}}(t) = \begin{pmatrix} \varrho_{aa} & \varrho_{as} \\ \varrho_{as}^* & \varrho_{ss} \end{pmatrix} = \frac{1}{2} [P_0 \sigma_0 + \mathbf{P} \cdot \boldsymbol{\sigma}]. \quad (2.9)$$

where P_0 and $\mathbf{P} = (P_x, P_y, P_z)$ are expansion coefficients referred to as the polarization vectors and $\sigma_0 = \mathbf{1}$ is the identity matrix. Since the diagonal components of the density matrix correspond to the distribution functions for the active-mixed and sterile neutrinos, we have

$$f_{\nu_a} = \frac{1}{2}(P_0 + P_z), \quad f_{\nu_s} = \frac{1}{2}(P_0 - P_z). \quad (2.10)$$

The QKE (Eq. (2.3)) is rewritten with polarization vectors as

$$\dot{\mathbf{P}} = \vec{\mathcal{H}} \times \mathbf{P} - D(P_x \mathbf{x} + P_y \mathbf{y}) + \dot{P}_0 \mathbf{z}, \quad (2.11)$$

$$\dot{P}_0 = R_{\nu_a}, \quad (2.12)$$

where $\vec{\mathcal{H}} = (\mathcal{H}_x, \mathcal{H}_y, \mathcal{H}_z)$ is the neutrino Hamiltonian. We define $P_{\nu_a} \equiv P_0 + P_z$ and $P_{\nu_s} \equiv P_0 - P_z$ and rewrite the above equation into

$$\dot{P}_{\nu_a} = \mathcal{H}_x P_y + R_{\nu_a}, \quad (2.13)$$

$$\dot{P}_{\nu_s} = -\mathcal{H}_x P_y, \quad (2.14)$$

$$\dot{P}_x = -\mathcal{H}_z P_y - D P_x, \quad (2.15)$$

$$\dot{P}_y = \mathcal{H}_z P_x - \frac{1}{2} \mathcal{H}_x (P_{\nu_a} - P_{\nu_s}) - D P_y. \quad (2.16)$$

Given the squared-mass difference between the mass eigenstates $\delta m^2 \equiv m_2^2 - m_1^2$ and the mixing angle in a vacuum θ , each component of the neutrino Hamiltonian is explicitly expressed as

$$\mathcal{H}_x = \frac{\delta m^2}{2p} \sin 2\theta, \quad (2.17)$$

$$\mathcal{H}_y = 0, \quad (2.18)$$

$$\mathcal{H}_z = -\frac{\delta m^2}{2p} \cos 2\theta + \mathcal{H}_{\text{mat}}. \quad (2.19)$$

The matter effect appears as the potential term \mathcal{H}_{mat} , which can be written as

$$\begin{aligned} \mathcal{H}_{\text{mat}} &= -\frac{8\sqrt{2}}{3} G_{\text{F}} p \left[\frac{\rho_e}{m_W^2} + \frac{\rho_{\nu_a}}{m_Z^2} \right], \\ &= -\frac{4\sqrt{2}}{3\pi^2} G_{\text{F}} p \left[\frac{g_e}{m_W^2} \int_0^\infty dp' p'^2 \frac{E_e}{\exp(E_e/T_\gamma) + 1} + \frac{g_\nu}{m_Z^2} \int_0^\infty dp' p'^3 f_{\nu_a} \right]. \end{aligned} \quad (2.20)$$

In the above expression, T_γ is the photon temperature, and $E_e = \sqrt{p^2 + m_e^2}$ is the energy of electrons. Also, $g_e = 4$ is the statistical degree of freedom of electrons and $g_\nu = 2$ is that for

each flavor of neutrinos. The first and second terms in the bracket correspond to the charged- and neutral-current interactions of ν_e with electrons, respectively.

The active-spectator neutrinos ν_{sp} are irrelevant to the neutrino oscillation. Therefore, their time evolution can be described by the momentum-dependent classical Boltzmann equation:

$$\frac{df_{\nu_{\text{sp}}}(t)}{dt} = \left(\frac{\partial}{\partial t} - H p \frac{\partial}{\partial p} \right) f_{\nu_{\text{sp}}}(t) = C[f_{\nu_{\text{sp}}}(t), t], \quad (2.21)$$

where $f_{\nu_{\text{sp}}}$ is the distribution function of the active-spectator neutrino, and $C[f_{\nu_{\text{sp}}}(t), t]$ is the collision term for ν_{sp} , whose expression is given by the same equation as the production rate for ν_a , but with $f_{\nu_{\text{sp}}}$.

In order to calculate the thermalization of active and sterile neutrinos in the expanding Universe, it is necessary to solve the Friedman equation,

$$H \equiv \frac{\dot{a}}{a} = \sqrt{\frac{8\pi G\rho}{3}}, \quad (2.22)$$

to give the time evolution of the scale factor $a(t)$. The total energy density ρ is written as

$$\begin{aligned} \rho &= \rho_\gamma + \rho_e + \rho_\nu + \rho_\phi \\ &= \frac{\pi^2}{15} T_\gamma^4 + \frac{g_e}{2\pi^2} \int_0^\infty dp p^2 \frac{E_e}{\exp(E_e/T_\gamma) + 1} \\ &\quad + \frac{g_\nu}{2\pi^2} \int_0^\infty dp p^3 (f_{\nu_a} + 2f_{\nu_{\text{sp}}} + f_{\nu_s}) + \rho_\phi. \end{aligned} \quad (2.23)$$

In the above expression, ρ_γ , ρ_e , ρ_ν , and ρ_ϕ are the energy densities of photons, electrons, neutrinos, and the parent particle, respectively. All flavors of neutrinos contribute to the total energy density of neutrinos, *i.e.* $\rho_\nu = \rho_{\nu_a} + \rho_{\nu_{\text{sp}}} + \rho_{\nu_s}$.

The evolution of ρ_ϕ can be obtained by solving the integrated Boltzmann equation for ϕ :

$$\frac{d\rho_\phi}{dt} = -\Gamma_\phi \rho_\phi - 3H\rho_\phi, \quad (2.24)$$

where Γ_ϕ is the decay rate of ϕ , and the lifetime of ϕ is given by its inverse, *i.e.* $\tau_\phi = \Gamma_\phi^{-1}$. This equation can be integrated analytically for the non-relativistic particle ϕ , and we obtain

$$\frac{\rho_\phi}{s} = \frac{\rho_{\phi,0}}{s_0} e^{-\Gamma_\phi t}, \quad (2.25)$$

where $\rho_{\phi,0}$ and s_0 are the energy density of ϕ and the total entropy density at the initial time t_0 , respectively. In Eq. (2.25), we have assumed $\rho_{\phi,0}$ dominates the energy densities of other background particles, *i.e.* $\rho_{\phi,0} \gg (\rho_\gamma + \rho_e + \rho_\nu)_{t=t_0}$.

The energy and entropy injected from the decay of the parent particle ϕ during reheating are taken into account by solving the energy conservation equation:

$$\frac{d\rho}{dt} = -3H(\rho + P). \quad (2.26)$$

The total pressure P can be expressed as

$$\begin{aligned} P &= P_\gamma + P_e + P_\nu \\ &= \frac{\pi^2}{45} T_\gamma^4 + \frac{g_e}{6\pi^2} \int_0^\infty dp \frac{p^4}{E_e \exp(E_e/T_\gamma) + 1} \\ &\quad + \frac{g_\nu}{6\pi^2} \int_0^\infty dp p^3 (f_{\nu_a} + 2f_{\nu_{sp}} + f_{\nu_s}). \end{aligned} \quad (2.27)$$

Since all electromagnetic particles are instantaneously thermalized during reheating, they have a common temperature T_γ . Hence, we can rewrite Eq. (2.26) into the differential equation for the time evolution of T_γ :

$$\frac{dT_\gamma}{dt} = - \frac{-\Gamma_\phi \rho_\phi + 4H(\rho_\gamma + \rho_\nu) + 3H(\rho_e + P_e) + \frac{d\rho_\nu}{dt}}{\frac{\partial \rho_\gamma}{\partial T_\gamma}|_{a(t)} + \frac{\partial \rho_e}{\partial T_\gamma}|_{a(t)}}, \quad (2.28)$$

where Γ_ϕ and T_{RH} are uniquely related through the relation:

$$\Gamma_\phi = 3H(T_{\text{RH}}). \quad (2.29)$$

The energy density is dominated by radiation after reheating, and hence the Hubble expansion rate can be written as

$$H = \sqrt{\frac{g^* \pi^2}{90} \frac{T_{\text{RH}}^2}{m_{\text{pl}}}}, \quad (2.30)$$

where $m_{\text{pl}} \sim 2.4 \times 10^{18}$ GeV is the reduced Planck mass, and $g^* = 10.75$ is the canonical value of the relativistic degrees of freedom at the cosmic temperature of $\mathcal{O}(1)$ MeV. Substituting Eq. (2.30) into Eq. (2.29) yields the one-to-one correspondence between the reheating temperature and the lifetime of the parent particle ϕ :

$$T_{\text{RH}} \sim 0.7 \text{ MeV} \left(\frac{\Gamma_\phi}{\text{sec}^{-1}} \right)^{1/2}. \quad (2.31)$$

This gives a reasonable estimate of the cosmic temperature at which the radiation-dominated epoch attains.

The results of the thermalization of active and sterile neutrinos are obtained by simultaneously solving Eqs. (2.13)–(2.16), (2.21), (2.22), (2.25), (2.28). For this purpose, we use the LASAGNA code [18, 46], which is an efficient ordinary differential equation solver optimized for the sterile neutrino production in the early Universe, with suitable modifications. Also, we utilize the SuperLU MT package [49, 50] to make use of the multicore CPU servers for numerical performance.

III. NUMERICAL RESULT: STERILE NEUTRINO THERMALIZATION

The abundance of neutrinos is often described in terms of the effective number of neutrino species N_{eff} . In the case of ν_e - ν_s mixing, it is defined as

$$N_{\text{eff}} = N_{\text{eff},\nu_a} + N_{\text{eff},\nu_s} + 2 N_{\text{eff},\nu_{\text{sp}}} = \rho_{\nu_a}/\rho_{\nu_{\text{std}}} + \rho_{\nu_s}/\rho_{\nu_{\text{std}}} + 2 \rho_{\nu_{\text{sp}}}/\rho_{\nu_{\text{std}}}, \quad (3.1)$$

where $N_{\text{eff},\nu_\alpha}$ ($\alpha = e, s, \text{sp}$) is the contribution of each neutrino species to the total N_{eff} , and $\rho_{\nu_{\text{std}}}$ is the energy density of one species of neutrinos in the standard big-bang model.⁵ The factor of two in front of $N_{\text{eff},\nu_{\text{sp}}}$ accounts for the contribution from ν_μ and ν_τ . By definition, $N_{\text{eff},\nu_\alpha} = 1$ corresponds to the full thermalization of ν_α , *i.e.* the energy spectrum of ν_α can be expressed as the thermal (Fermi-Dirac) distribution.

Figure 1 shows the relation between the reheating temperature T_{RH} and the effective number of the neutrino species N_{eff} . The mass difference δm^2 and the mixing angle θ between the active and sterile neutrinos are fixed to $(\delta m^2, \sin^2 2\theta) = (1.29 \text{ eV}^2, 0.035)$, which is the best-fit value obtained from data analysis of ν_e disappearance experiments in Ref. [51]. In the figure, both N_{eff} and $N_{\text{eff},\nu_\alpha}$ increase with T_{RH} since the active neutrino production via $e^- + e^+ \rightarrow \nu_\alpha + \bar{\nu}_\alpha$ is more efficient at a higher temperature, and neutrinos have more time to be produced during reheating. The abundance of sterile neutrinos decreases for $T_{\text{RH}} < T_{\text{max}}$ ($\sim 13 \text{ MeV}$ for $m_s \sim 1 \text{ eV}$) and vanishes at $T_{\text{RH}} < 1 \text{ MeV}$ due to the decoupling of active neutrinos from the thermal plasma. An inequality $N_{\text{eff},\nu_a} > N_{\text{eff},\nu_{\text{sp}}}$ always holds because the neutrino interaction with the background electrons is stronger for ν_e than ν_μ or ν_τ . The figure also reveals that the neutrino self-interaction enhances the production efficiency of the sterile neutrino. This is because the neutrino self-interaction increases the collisional-damping rate D and increase the effective production rate of sterile neutrinos, which approximately scales as $D \sin^2 2\theta_M$, where θ_M is the mixing angle in a medium [52]. The effect of the neutrino self-interaction was neglected in Ref. [34], or approximately considered in Refs. [30, 32, 33].

Figure 2 shows the time evolution of $N_{\text{eff},\nu_\alpha}$ for typical values of T_{RH} . The competition between the dilution of neutrinos due to the entropy production induced by the decay of ϕ and the production of neutrinos determines the behavior of $N_{\text{eff},\nu_\alpha}$. Since neutrinos are only weakly produced in the thermal bath of photons and electrons, the former is dominant for $T_\gamma > T_{\text{RH}}$, and the effect takes its maximum at $T_\gamma \sim T_{\text{RH}}$, when the cosmic time is comparable to the lifetime of

⁵ Here we normalize the contribution of ν_α ($\alpha = e, \mu, \tau$) to the effective number of neutrino species $N_{\text{eff},\nu_\alpha}$ in units of the energy density of ν_e in the standard big-bang model, $\rho_{\nu_{e,\text{std}}}$. Another choice for the normalization is to take the standard energy density of ν_μ or ν_τ , but the difference between $\rho_{\nu_\alpha}/\rho_{\nu_{e,\text{std}}}$ and $\rho_{\nu_\alpha}/\rho_{\nu_{\mu,\text{std}}}$ (or $\rho_{\nu_\alpha}/\rho_{\nu_{\tau,\text{std}}}$) should be quite small ($< 1\%$), and hence negligible. The difference in N_{eff} due to its definition is therefore irrelevant to our final results.

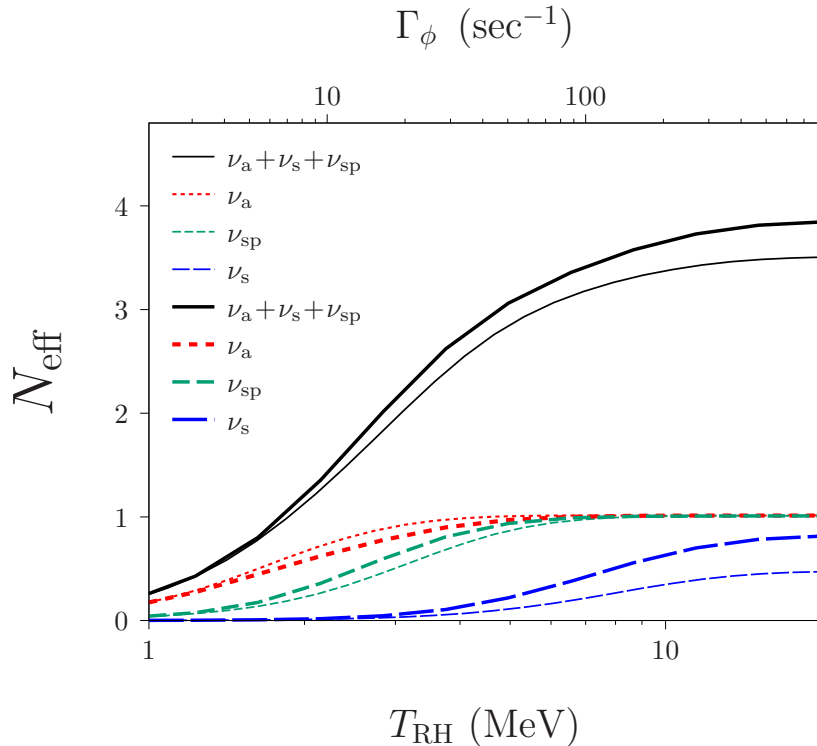


FIG. 1. Effective number of neutrino species $N_{\text{eff}} = N_{\text{eff}, \nu_a} + N_{\text{eff}, \nu_s} + 2 N_{\text{eff}, \nu_{\text{sp}}}$ as a function of the reheating temperature T_{RH} , for the case of ν_e - ν_s mixing. The narrow (bold) line corresponds to the case without (with) the neutrino self-interaction. The black line is for N_{eff} , whereas the red, green, and blue lines are for N_{eff, ν_a} , $N_{\text{eff}, \nu_{\text{sp}}}$, and N_{eff, ν_s} , respectively.

ϕ . This leads the local minimum of $N_{\text{eff}, \nu_\alpha}$ in Fig. 2. For $T_\gamma < T_{\text{RH}}$, neutrino production becomes dominant compared to the dilution effect, which is negligible after the decay of ϕ . The value of $N_{\text{eff}, \nu_\alpha}$ increases for $T_\gamma < T_{\text{RH}}$ until neutrinos decouple from other particles at around $T_\gamma \sim 1$ MeV. This explains the behavior of the time evolution of N_{eff} . Also, Fig. 2 shows that eV-scale sterile neutrinos start to be produced through neutrino oscillation at around $T_\gamma \sim 13$ MeV ($= T_{\text{max}}$), as discussed in the previous section (see Eq. (2.1)).

In Fig. 3, we plot the energy spectrum of each flavor of neutrinos for the typical values of T_{RH} . We evaluate the spectra at $T_\gamma = 10^{-2}$ MeV, which is much later than the electron-pair annihilation and the neutrino decoupling. It can be seen from Fig. 3 that a peak position of the neutrino energy spectra is shifted to lower than $p/T_\gamma \sim 3.15$, which corresponds to the thermal value for fermions. This is because the photon temperature T_γ increases by a factor of $(11/4)^{1/3} \sim 1.4$ compared to those of neutrinos after the annihilation of electrons.

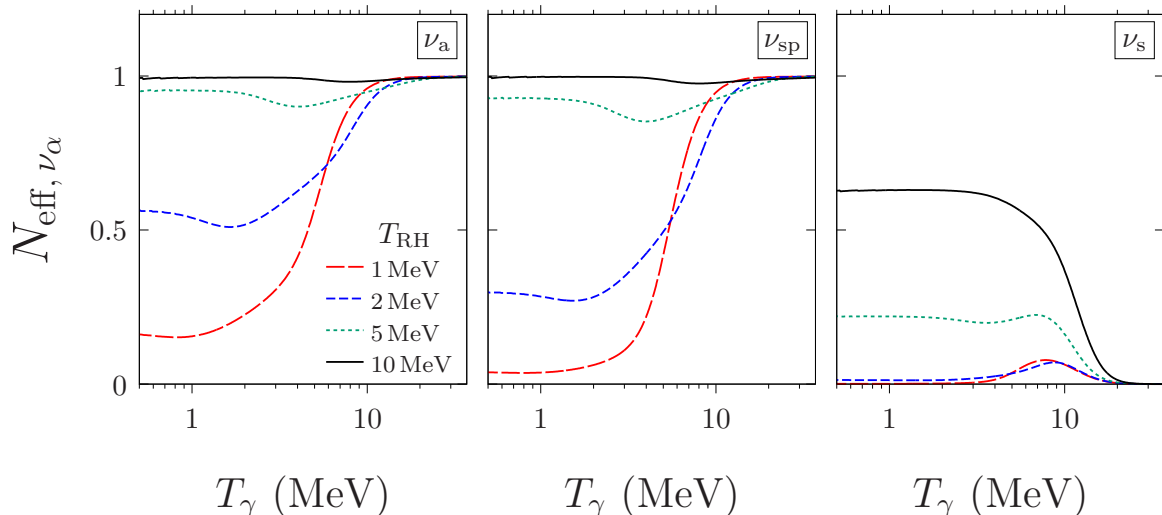


FIG. 2. Temperature evolution of $N_{\text{eff}, \nu_\alpha}$ ($\alpha = a, s, \text{sp}$), for the case of ν_e - ν_s mixing. The left panel is for N_{eff, ν_a} , the middle panel is for $N_{\text{eff}, \nu_{\text{sp}}}$, and the right panel is for N_{eff, ν_s} . In each panel, the red long-dashed line is for $T_{\text{RH}} = 1$ MeV, the blue middle-dashed line is for $T_{\text{RH}} = 2$ MeV, the green short-dashed line is for $T_{\text{RH}} = 5$ MeV, and the black solid line is for $T_{\text{RH}} = 10$ MeV.

The averaged energy of neutrinos is expressed by the distortion parameter $R_{\text{dist}, \nu_\alpha}$, defined by

$$R_{\text{dist}, \nu_\alpha} = \frac{1}{3.15 T_{\nu_\alpha, \text{eff}}} \frac{\rho_{\nu_\alpha}}{n_{\nu_\alpha}}, \quad (3.2)$$

where $T_{\nu_\alpha, \text{eff}} (= [4\pi^2 n_{\nu_\alpha} / 3\zeta(3)]^{1/3})$ is the effective temperature for each flavor of neutrinos. The thermal spectrum corresponds to $R_{\text{dist}, \nu_\alpha} = 1$ by definition. In Fig. 4, we show the dependence of the distortion parameter R_{dist} on the reheating temperature. The figure reveals that R_{dist} increases as the reheating temperature decreases, and particularly it goes to unity for active neutrinos at $T_{\text{RH}} > 10$ MeV. The production mechanism of active neutrinos is responsible for this feature. Active neutrinos are produced only from the electron-pair annihilation, and each neutrino in the final state has energy larger than the electron mass $m_e \sim 0.5$ MeV. Therefore, the value of $R_{\text{dist}, \nu_\alpha}$ becomes larger than unity due to the large contribution from neutrinos produced when the electron is still relativistic. The scattering rate of the process $e^\pm + \nu_\alpha \rightarrow e^\pm + \nu_\alpha$ ($\alpha = a, s, \text{sp}$), is not sufficient to fully equilibrate the neutrino spectrum since it is of the order of $\mathcal{O}(G_F^2)$, which is the same as that of the neutrino-pair production. As seen in Fig. 4, the distortion parameter for the spectator neutrino is always larger than that of the active-mixed neutrino since we consider the mixing between ν_e and ν_s . The scattering between the background electron and the electron neutrino is more frequent than those of the other active neutrino species. Also, the energy spectrum of sterile

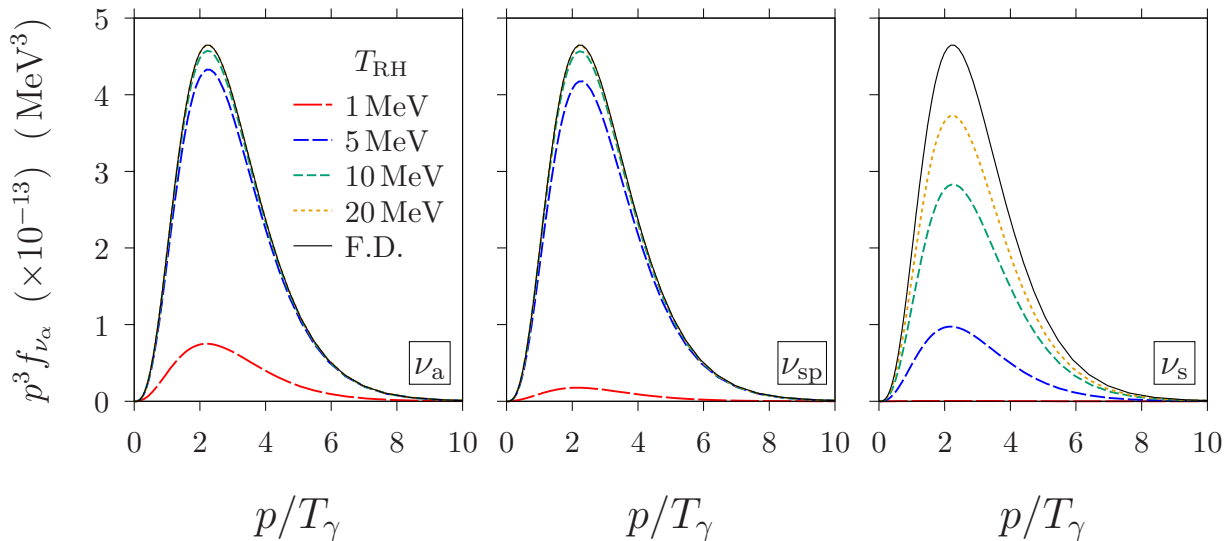


FIG. 3. Dependence of the final energy spectra of neutrinos on the reheating temperature, evaluated at $T_\gamma = 10^{-2}$ MeV, for the case of ν_e - ν_s mixing. The effect of the neutrino self-interaction is included in the calculation. The x -axis is the neutrino energy p divided by the photon temperature T_γ , and the y -axis is the differential energy spectrum of neutrinos. The left panel is for ν_a , the middle panel is for ν_{sp} , and the right panel is for ν_s . In each panel, the red long-dashed line is for $T_{RH} = 1$ MeV, the blue middle-dashed line is for $T_{RH} = 5$ MeV, the green short-dashed line is for $T_{RH} = 10$ MeV, and the black solid line is for $T_{RH} = 20$ MeV. In the left and middle panels, the spectrum for $T_{RH} = 20$ MeV is almost the same as that of the Fermi-Dirac distribution $f_{FD} = 1/\exp[p/T_\nu + 1]$, where $T_\nu = (4/11)^{1/3} T_\gamma \sim T_\gamma/1.4$.

neutrinos is heavily distorted compared to active neutrinos since electrons do not interact with sterile neutrinos. We note that the value of $R_{\text{dist}, \nu_s} (\sim 1.6)$ for $T_{RH} = 5$ MeV is $\mathcal{O}(10)\%$ larger than that obtained in Ref. [32], $R_{\text{dist}, \nu_s} \sim 1.3$. This is possibly due to assumptions which they adopted to simplify the thermalization calculation of sterile neutrinos, namely the sterile neutrino abundance is negligible compared to the thermal abundance $f_{\nu_s} \ll f_{FD} = 1/\exp[p/T_\gamma + 1]$, and the sterile neutrino production only takes place at $T_\gamma < T_{RH}$.

Figure 5 shows the mass dependence of N_{eff} . As can be seen from Fig. 5, the mass dependence is negligible for $T_{RH} \sim \mathcal{O}(1)$ MeV, which justifies the assumption in Ref. [34]. The reason is that the matter effect is almost negligible at a low temperature of $\mathcal{O}(1)$ MeV, and the effective production rate of the sterile neutrino is therefore given by $\sim D \sin^2 2\theta$ for both cases of $m_s = 1$ eV and 1 keV. The damping rate D is associated only with active neutrinos, and it has no sensitivity to the sterile neutrino property.

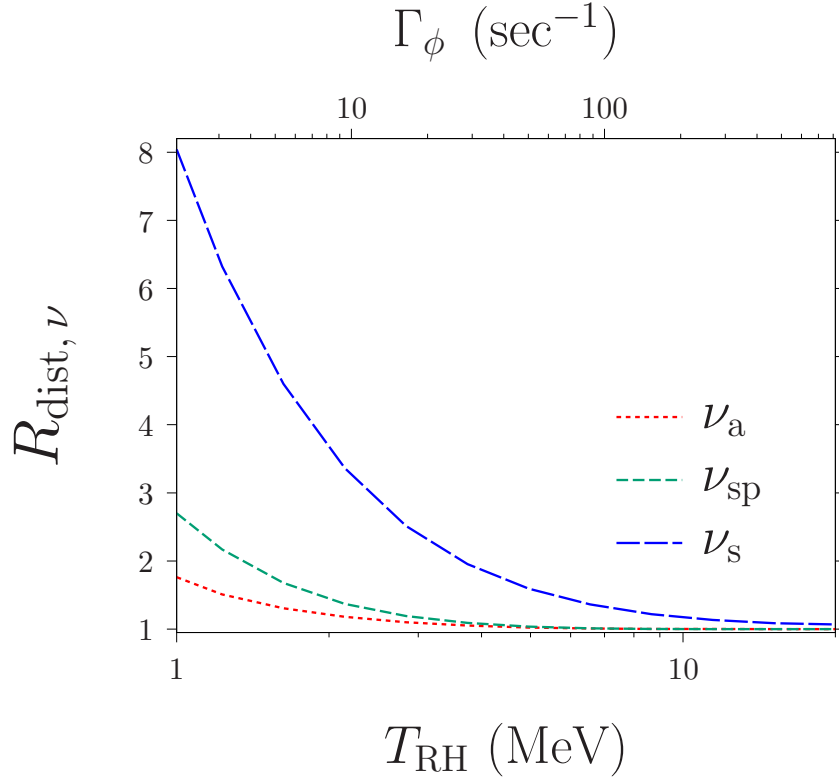


FIG. 4. Dependence of the distortion parameter for each flavor of neutrinos $R_{\text{dist}, \nu_\alpha}$ ($\alpha = a, s, \text{sp}$) on the reheating temperature T_{RH} , for the case of $\nu_e - \nu_s$ mixing. The red short-dashed line is for ν_a , the green middle-dashed line is for ν_{sp} , and the blue long-dashed line is for ν_s . $R_{\text{dist}} = 1$ corresponds to the thermal Fermi-Dirac spectrum.

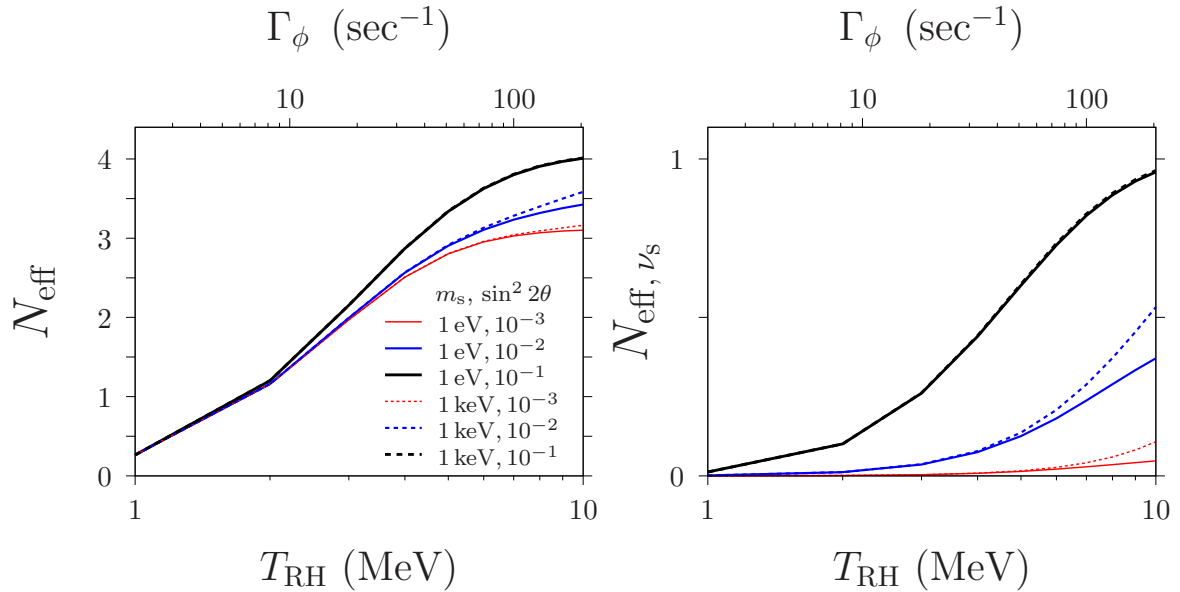


FIG. 5. Mass dependence of the effective number of neutrino species for all flavors of neutrinos (left) and sterile neutrinos (right) for each value of the active-sterile mixing $\sin^2 2\theta$, for the case of ν_e - ν_s mixing. The solid lines are for $m_s = 1$ eV, while dashed lines are for $m_s = 1$ keV. The red, blue, and black lines correspond to $\sin^2 2\theta = 10^{-3}$, 10^{-2} , and 10^{-1} , respectively. There are no apparent mass dependences for the cases of $\sin^2 2\theta = 10^{-1}$.

IV. NUMERICAL RESULT: BIG BANG NUCLEOSYNTHESIS

The thermalization of neutrinos is closely associated with BBN. In this section, we introduce the formalism for the calculation of BBN after a brief introduction to the role of neutrinos in BBN. For the detail of the theoretical framework, we refer the reader to Ref. [37]. The numerical results of the BBN calculation in cosmological models with MeV-scale reheating temperature is presented in the latter part of this section.

A. Neutrino thermalization and neutron-to-proton ratio

Neutrinos affect the light-element abundances synthesized in BBN since they are involved in the exchange reactions between protons and neutrons:

$$n \leftrightarrow p + e^- + \bar{\nu}_e, \quad (4.1a)$$

$$e^+ + n \leftrightarrow p + \bar{\nu}_e, \quad (4.1b)$$

$$\nu_e + n \leftrightarrow p + e^-, \quad (4.1c)$$

which set the neutron-to-proton ratio (n/p) before the nucleosynthesis. The neutron-to-proton ratio is one of the most important parameters in BBN, which determines the final abundances of light elements. In particular, the mass fraction of ${}^4\text{He}$, which is denoted as Y_p , is written in a simple analytical form of $Y_p \sim 1/\{1 + (n/p)_{\text{bbn}}^{-1}\}$. The neutron-to-proton ratio $(n/p)_{\text{bbn}}$ is the value just before the deuterium bottleneck opens and the synthesis of light elements becomes effective, which corresponds to the cosmic time of $t_{\text{bbn}} \sim 200$ sec (or the temperature of $T_{\text{bbn}} \sim 80$ keV). The freeze-out value of the ratio $(n/p)_f$ is related to $(n/p)_{\text{bbn}}$ as

$$(n/p)_{\text{bbn}} = (n/p)_f e^{-t_{\text{bbn}}/\tau_n}, \quad (4.2)$$

where $\tau_n = 880.2 \pm 1.0$ sec (68% C.L.) is the neutron lifetime [41]. The freeze-out value is $(n/p)_f \sim 1/6$ in the standard big-bang model, where all active neutrinos are fully thermalized well-before BBN, and hence $(n/p)_{\text{bbn}} \sim 1/7$ and $Y_p \sim 0.25$ [41].

As discussed in Secs. II and III, neutrinos are not completely thermalized in cosmological models with MeV-scale reheating temperature. The incomplete thermalization of neutrinos changes both the freeze-out of the processes (4.1a)–(4.1c) and the Hubble expansion rate. Therefore, we expect a different $(n/p)_f$ value from that attained in the standard big-bang model in this case. Refs. [53, 54] provided a comprehensive discussion of the mechanism. The abundances of the other light elements

such as D, ^3He , ^6Li , and ^7Li are very sensitive to the production abundance of ^4He , which is the second most abundant element in the Universe. Consequently, light-element abundances in the low-reheating scenario are different from those of the standard big-bang model. Also, among the neutrino species only ν_e is relevant to the processes (4.1a)–(4.1c). For that reason, light-element abundances are highly sensitive to the ν_e spectrum, and any physics changing the neutrino flavors in the early Universe such as the neutrino self-interaction and neutrino oscillation plays an important role in the synthesis of light elements.

B. Observational abundances

The abundances of deuterium and helium in the current Universe are measured with $\mathcal{O}(1)\%$ accuracy. The baryon-to-proton ratio η_B , which is the only free parameter of the standard theory of BBN, is also determined with high precision using these measurements [41]. In this study, we adopt the primordial mass fraction of ^4He reported in Ref. [55]:

$$Y_p = 0.2449 \pm 0.0040 \quad (68\% \text{ C.L.}), \quad (4.3)$$

which was obtained from the observation of the recombination line of metal-poor stars in the extra-galactic HII regions or blue compact galaxies.⁶ For deuterium, we adopt [57]

$$\text{D}/\text{H} = (2.545 \pm 0.025) \times 10^{-5} \quad (68\% \text{ C.L.}), \quad (4.4)$$

which was determined using the absorption spectra in high-redshift metal-poor quasar absorption systems.⁷

C. Numerical calculation

We numerically solve the code of the reaction network for light elements based on the Kawano code [59] with the updated nuclear reaction rates reported in Refs. [60–64] (see Ref. [65] for more details). The contribution of ϕ is accounted for in the Friedman equation, Eq. (2.22), and the energy conservation equation, Eq. (2.26). Also, we pre-evaluate the energy densities of active and sterile neutrinos together with weak reaction rates of the processes (4.1a)–(4.1c) with the LASAGNA code

⁶ A slightly large value of the ^4He abundance was reported in Ref. [56], $Y_p = 0.2551 \pm 0.0022$ (68% C.L.). Since the authors of Ref. [55] reanalyzed the same dataset used in Ref. [56], it should be reasonable to adopt the value reported in Ref. [55].

⁷ The authors of Ref. [58] reported $\text{D}/\text{H} = (2.527 \pm 0.030) \times 10^{-5}$ (68% C.L.), which is similar to (4.4). Since the difference of the mean values between this value and (4.4) falls within a $1\text{-}\sigma$ error, our result does not change even if we adopted this value to be the primordial D/H.

and interpolate the data in the BBN code. In the standard BBN, the baryon-to-photon ratio η_B is the only free parameter of the theory. Currently, the value of η_B is precisely determined from the observation of CMB in the Planck collaboration [47]. In this study, we adopt the Planck bound on η_B for the base Λ CDM model extended by two additional parameters, namely the effective number of neutrino species, N_{eff} , and the effective mass of sterile neutrinos, m_s^{eff} :⁸

$$\eta_B = (6.14 \pm 0.04) \times 10^{-10} \quad (68\% \text{ C.L.}), \quad (4.5)$$

as a prior for the calculation of BBN.

The light-element abundance is sensitive to the decay mode of the parent particle ϕ [37, 54, 66]. In this study, we assume that the parent particle ϕ decays into both radiation (*i.e.* photons and charged leptons) and hadrons (*i.e.* quarks and gluons) as in Refs. [37, 54]. For the case of the direct decay of the parent particle into active neutrino pairs $\phi \rightarrow \nu_\alpha + \bar{\nu}_\alpha$ ($\alpha = e, \mu, \tau$), see Ref. [66].

The effect of the particle injection from the parent particle ϕ is more significant in the case where the hadronic branching ratio $B_h \neq 0$. In the case where the parent particle decays exclusively into radiation, the thermal bath of photons and electrons is instantaneously produced by cascade reactions through electromagnetic interaction, and active neutrinos are gradually produced from the thermal bath through the weak interaction. For $B_h \neq 0$, mesons, baryons, and their anti-particles are copiously produced from quarks and gluons after the hadronization, and they induce additional exchange reactions between neutrons and protons. Consequently, it affects the freeze-out value of the neutron-to-proton ratio $(n/p)_f$ and leads to different outcomes of BBN [37, 54, 67]. In our calculation, we take into account the hadronic effect induced by charged pions (π^\pm) and nucleons (n, \bar{n}, p, \bar{p}) injected from the decay of ϕ and neglect the effect of other hadronic particles for conservative treatment. We use the thermal reaction rates for the hadronic processes interchanging neutrons and protons. This treatment is justified since most of the injected hadrons are instantaneously stopped by inverse Compton-like scattering or Coulomb interaction with background particles (*i.e.* mainly photons and electrons) and reach equilibrium [68, 69]. Also, we evaluate the number of hadrons produced in the hadronic decay using the Pythia 8.2 code [70, 71], assuming the decays of ϕ into the $u\bar{u}$ pair as a specific process for the quark production.

Figure 6 shows the abundances of helium (Y_p) and deuterium (D/H) as a function of the reheating temperature T_{RH} for the 100% radiative decay cases. The mixing parameters of sterile neutrinos are fixed to the best-fit values in Ref. [51], as in the previous section. Also, the baryon-

⁸ The thermalization of neutrinos and light-element abundances affect the recombination, and this is therefore an approximate treatment. Ref. [47] assumes that three-flavors of active neutrinos are completely thermalized and adopt the value of Y_p in the standard big-bang model.

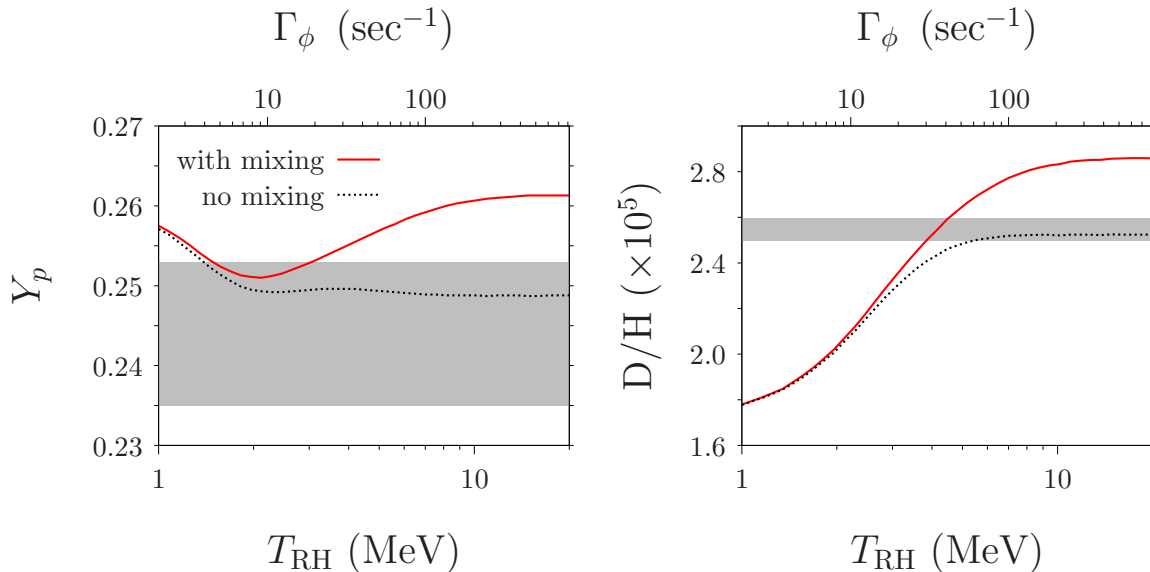


FIG. 6. Mass fraction of ${}^4\text{He}$, Y_p , and the deuterium-to-hydrogen ratio, D/H , as functions of the reheating temperature T_{RH} for the cases corresponding to the 100% radiative decay of the parent particle ϕ , with the assumption of $\nu_e\text{-}\nu_s$ mixing. The value of the baryon-to-photon ratio is fixed to $\eta_B = 6.14 \times 10^{-10}$ in the figure. The red solid line is for sterile neutrinos with the best-fit mixing parameters $(\delta m^2, \sin^2 2\theta) = (1.29 \text{ eV}^2, 0.035)$ reported in Ref. [51], and the case without sterile neutrinos is plotted by the black dotted line for reference. The $2\text{-}\sigma$ observational bounds on Y_p (Ref. [55]) and D/H (Ref. [57]) are also shown by the gray-shaded regions.

to-photon ratio η_B is set to be the median value of Eq. (4.5). As seen in Fig. 6, the light-element abundance increases with the reheating temperature. This is because sterile neutrinos are more abundantly produced for a large T_{RH} (see Fig. 1), and therefore the expansion rate H increases. This leads to the early decoupling of the exchange reactions between protons and neutrons (4.1a)–(4.1c). Consequently, the freeze-out temperature T_c increases and more neutrons remain unburnt, which increases $(n/p)_f$ and light-element abundances, *i.e.* Y_p and D/H . In Fig. 6, a similar dependence of Y_p and D/H on the reheating temperature can be seen even for the case without sterile neutrinos. For small T_{RH} an incomplete thermalization of active neutrinos decreases the expansion rate, and Y_p and D/H decrease due to the effect. The increase of Y_p for small T_{RH} is caused by a decrease in the weak rates responsible for the interconversion between protons and neutrons, Γ_{np} . This accelerates the decoupling of the processes (4.1a)–(4.1c) and plays a role in increasing the freeze-out value of the neutron-to-proton ratio $(n/p)_f$ and Y_p . The increase and decrease of Y_p due to small T_{RH} are competing, but the former dominates the latter for large T_{RH} and the opposite is true for small T_{RH} (see Refs. [37, 54] for more detail).

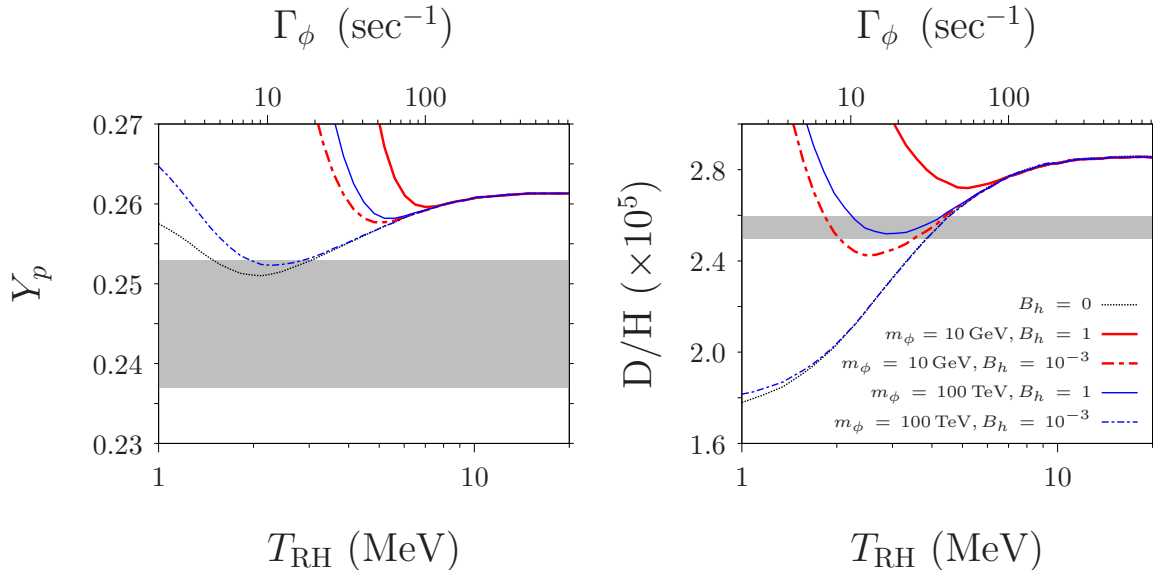


FIG. 7. Same as Fig. 6, but for the cases with the hadronic decay of the parent particle ϕ . The case of $B_h = 0$ (black dotted) corresponds to the 100% radiative decay of ϕ .

Figure 7 shows the results of the hadronic decay cases. It can be seen that light-element abundances increase for $T_{\text{RH}} \lesssim 10$ MeV due to the hadronic decay effect compared to those for the 100% radiative decay cases. This is because the injection of the high-energy hadrons induces additional exchange reactions between protons and neutrons, $p + N \leftrightarrow n + N'$, where N and N' are mesons or baryons, to equilibrate the number densities of protons and neutrons [37, 54, 67, 68]. This is not true for $T_{\text{RH}} \gtrsim 10$ MeV because the hadronic decay occurs much before the decoupling of the processes (4.1a)–(4.1c), and the neutron-to-proton ratio is subsequently equilibrated by the weak processes again, which erases the hadronic decay effect.

V. COSMOLOGICAL CONSTRAINT ON STERILE NEUTRINOS

In this section, we summarize the cosmological constraint on sterile neutrinos, especially focusing on the eV-scale sterile neutrinos motivated by the SBL anomaly. Refs. [30, 32, 33] have shown that cosmological observations place the most stringent bound on the existence of eV-scale sterile neutrinos. Here we summarize the latest results of cosmological observations of light elements and the CMB radiation as well as ground-based neutrino experiments.

A. Constraints from BBN

Sterile neutrinos affect the synthesis of light elements as discussed in Sec. IV. The BBN bound on sterile neutrinos can be obtained by requiring the agreement between theoretical predictions and observed abundances of light elements by performing a χ^2 analysis. In this study, a χ^2 function is defined as follows:

$$\chi^2 \equiv \chi_{D/H}^2 + \chi_{Y_p}^2 = \frac{\{(D/H)_{\text{th}} - (D/H)_{\text{obs}}\}^2}{\sigma_{D,\text{th}}^2 + \sigma_{D,\text{obs}}^2} + \frac{\{Y_{p,\text{th}} - Y_{p,\text{obs}}\}^2}{\sigma_{Y_p,\text{th}}^2 + \sigma_{Y_p,\text{obs}}^2}, \quad (5.1)$$

where $\chi_{D/H}^2$ and $\chi_{Y_p}^2$ are χ^2 functions for each of D/H and Y_p . We use the suffix “obs” and “th” to denote the “observational” and “theoretical”, respectively. Also, σ is the uncertainty of the light-element abundance. The theoretical prediction of light-element abundances is defined at each point on the three-dimensional grid of $(m_s, \sin^2 2\theta, T_{\text{RH}})$. The theoretical error on each grid point is estimated by propagating the experimental errors in the nuclear reaction rates, the free neutron lifetime, and the hadronic reaction rates in the Monte-Carlo calculation of BBN. For the thermal cross-sections of the hadronic reactions, we use the results in Ref. [67] and assume a 30% error in each cross-section. We define the region of 95% confidence level as a parameter space satisfying

$$\chi^2(m_s, \sin^2 2\theta, T_{\text{RH}}) < 5.991. \quad (5.2)$$

B. Constraints from CMB

Thermalized sterile neutrinos contribute to N_{eff} and affect the recombination. Searching the signature in the CMB spectra, the *Planck* collaboration derived an upper limit on the effective mass of sterile neutrinos m_s^{eff} [47]:

$$m_s^{\text{eff}} < 0.65 \text{ eV}. \quad (5.3)$$

As we assume an absence of the neutrino chemical potential, sterile neutrinos are non-resonantly produced through its mixing with active neutrinos by the Dodelson-Widrow mechanism. In this case, the physical mass m_s is related to the effective mass as $m_s^{\text{eff}} = m_s N_{\text{eff}, \nu_s}$, where N_{eff, ν_s} is the thermalization degree of sterile neutrinos.

Figure 8–10 summarize the constraints on sterile neutrinos in the parameter space of $(m_s, \sin^2 2\theta)$. Figure 8 corresponds to the case assuming the standard big-bang model, while Figs. 9 and 10 correspond to the low-reheating scenario assuming the 100% radiative and hadronic decays of the parent particle ϕ .⁹ In each figure, we also show the current and future sensitivities of the ground-based experiments. The region denoted by R is already excluded from the reactor experiments (R) [72–74]. In the future, KATRIN (KA) [75] and PTOLEMY (P for 10 mg-yr and P2 for 100 g-yr exposures) [76] will prove much smaller mixing angles. In these figures, we also show the 95% C.L. preferred regions of the sterile neutrino reported in Refs. [51] and [77]. Such sterile neutrinos that explain the SBL anomaly are excluded in the standard big-bang model from cosmological observations (Fig. 8), but the low reheating temperature scenario changes the picture. If all the energy of ϕ goes to radiation after the decay, such sterile neutrinos are still compatible with cosmological observations (Fig. 9), which is consistent with the previous studies with simplified treatments [30, 32–34]. In such a case, the production of sterile neutrinos is strongly suppressed, relaxing the BBN and CMB bounds. In contrast, if some part of the energy of ϕ goes to hadrons, injected hadrons induce additional interconversion between neutrons and protons, and the BBN bound gets more severe (Fig. 10), as we discussed in Sec. IV. We note that in Fig. 10 we intentionally choose the mass and the hadronic branching ratio of ϕ to make the effect of the hadronic decay clear. For a heavier ϕ , $m_\phi > 10$ GeV, or a smaller hadronic branching ratio, $B_h < 1$, the effect of the hadronic decay should be smaller (See Refs. [37, 54, 67] for further discussions).

In light of our results, the existence of the light sterile neutrino explaining the SBL anomaly is still compatible with the observations of BBN and CMB, although it depends on the reheating temperature T_{RH} , the mass of the parent particle m_ϕ , and the hadronic branching ratio B_h of the decay. In the future, such light sterile neutrinos could be detected by direct detection experiments of the cosmic neutrino background such as the PTOLEMY project [76]. Also, energy spectra of active neutrinos are sensitive to the reheating temperature as well as the mass and the mixing angle of sterile neutrinos. A direct detection of the cosmic neutrino background should bring us reliable

⁹ We refrain from plotting the result in the region with $m_s > 10^{-1}$ keV in the case of the standard big-bang model. This is because the peak production of sterile neutrinos with such a large mass occurs at or above 50 MeV (see Eq. (2.1)) and therefore collisions between neutrinos and muons or light mesons, which are not considered in our computation, are non-negligible in the mass region.

information on the values of these parameters, associated with the theory beyond the standard model of particle physics.

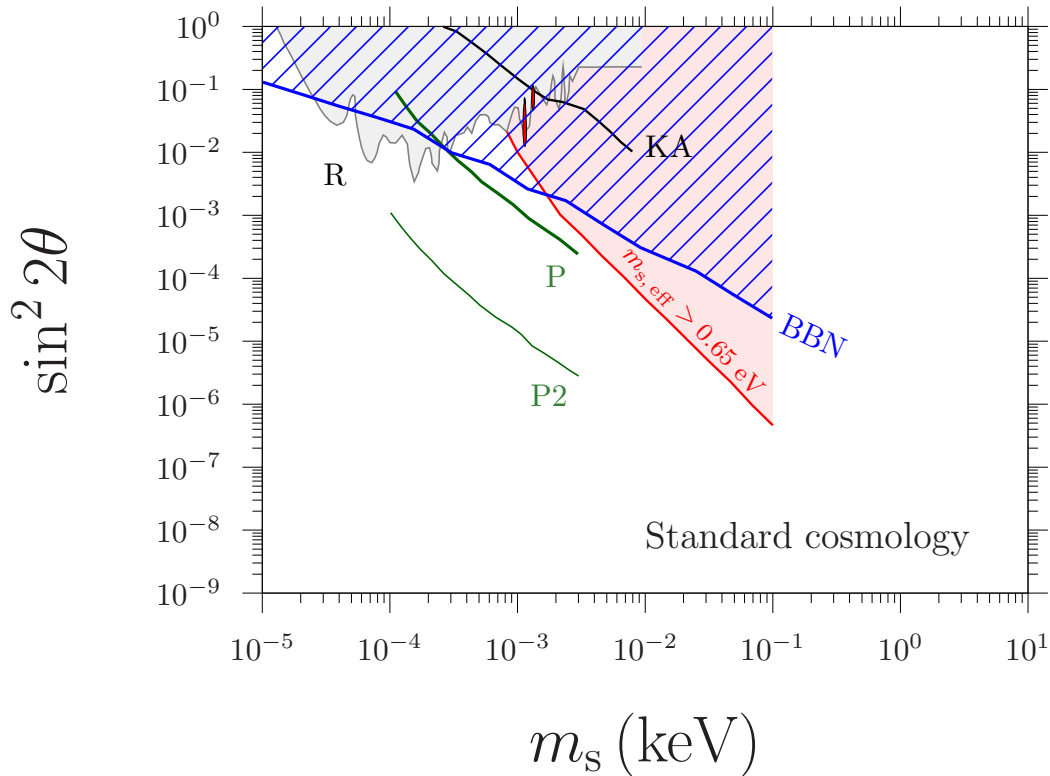


FIG. 8. Constraints on sterile neutrinos in the parameter space of $(m_s, \sin^2 2\theta)$ assuming the standard big-bang model, for the case of ν_e - ν_s mixing. The 95% C.L. bound based on the BBN calculation is shown by the blue-hatched region while that on the CMB by the red region. We fix the reheating temperature $T_{\text{RH}} = 5$ MeV to plot the CMB bound. Other excluded regions come from Daya Bay [72], Bugey-3 [73], and PROSPECT [74] (R, gray region), the KATRIN neutrino mass experiment (KA, solid-black line) [75]. The narrow vertically-long region colored in red corresponds to the best-fit region in the ν_e disappearance only (left, Ref. [51]) and the global (right, Ref. [77]) data analysis. The sensitivities with the future cosmic neutrino background experiment [74] are also shown (P and P2, green region).

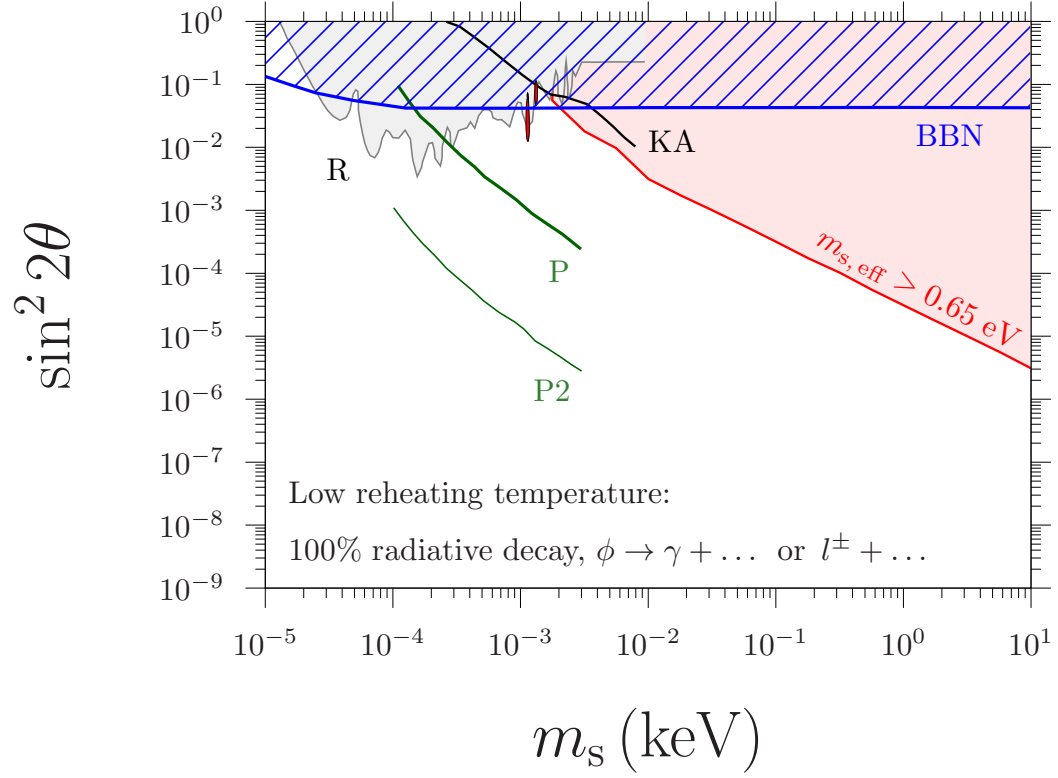


FIG. 9. The same as Fig. 8 but for the low reheating temperature case assuming 100% radiative decay of the parent particle ϕ .

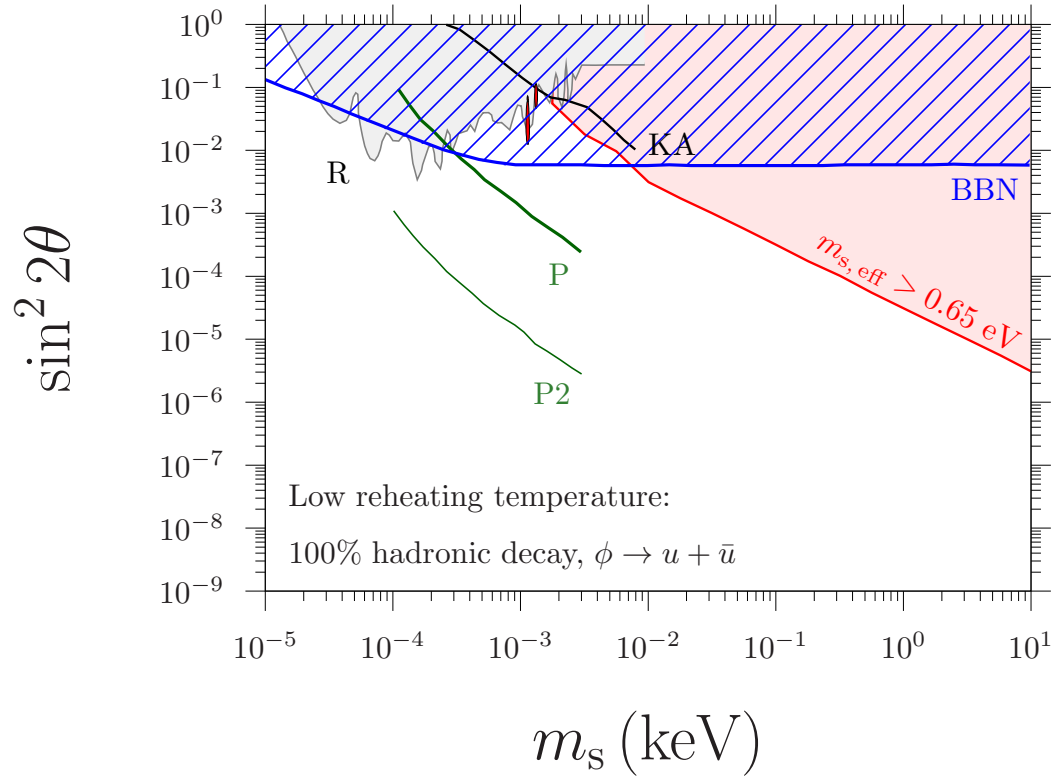


FIG. 10. The same as Fig. 9 but for the case corresponding to the 100% hadronic decay of the parent particle ϕ with $m_\phi = 10$ GeV. Compared to Fig. 9, the BBN bound is more severe and the preferred regions in Refs. [51] and [78] are excluded.

VI. CONCLUSIONS

We have investigated the cosmological production of light sterile neutrinos with masses and mixings consistent with those needed to explain the anomaly in short-baseline neutrino experiments, assuming a low reheating temperature of the Universe $T_{\text{RH}} \sim \mathcal{O}(1)$ MeV. Considering the sterile neutrino production through the combination of scatterings and non-resonant oscillations, we have numerically solved its evolution and found that the existence of such sterile neutrinos becomes consistent with Big Bang nucleosynthesis if the parent particle responsible for reheating decays exclusively into electromagnetically interacting radiation. In contrast, if the parent particle mainly decays into hadrons, the BBN bound gets tighter and the preferred regions for explaining the anomaly are excluded for a wide range of the mass and the hadronic branching ratio of the parent particle.

ACKNOWLEDGMENTS

Numerical computations were carried out on PC clusters at Center for Computational Astrophysics, National Astronomical Observatory of Japan (NAOJ) and Computing Research Center, High Energy Accelerator Research Organization (KEK). The work of NH has been partially supported by JSPS KAKENHI Grants No. JP19K23446. The work of KK has been supported by JSPS KAKENHI Grants No. JP17H01131, MEXT Grant-in-Aid for Scientific Research on Innovative Areas JP15H05889, JP18H04594, JP19H05114, and JP20H04750. The work of RSLH is supported by Danmarks Frie Forskningsfond (Project No. 8049-00038B).

-
- [1] LSND collaboration, *Evidence for $\nu(\mu) \rightarrow \nu(e)$ neutrino oscillations from LSND*, *Phys. Rev. Lett.* **81** (1998) 1774 [[nucl-ex/9709006](#)].
- [2] MINIBOONE collaboration, *Event Excess in the MiniBooNE Search for $\bar{\nu}_\mu \rightarrow \bar{\nu}_e$ Oscillations*, *Phys. Rev. Lett.* **105** (2010) 181801 [[1007.1150](#)].
- [3] MINIBOONE collaboration, *Observation of a Significant Excess of Electron-Like Events in the MiniBooNE Short-Baseline Neutrino Experiment*, [1805.12028](#).
- [4] DAYA BAY collaboration, *Measurement of the Reactor Antineutrino Flux and Spectrum at Daya Bay*, *Phys. Rev. Lett.* **116** (2016) 061801 [[1508.04233](#)].
- [5] DOUBLE CHOOZ collaboration, *Indication of Reactor $\bar{\nu}_e$ Disappearance in the Double Chooz Experiment*, *Phys. Rev. Lett.* **108** (2012) 131801 [[1112.6353](#)].
- [6] D. Abdurashitov et al., *The Russian-American gallium experiment (SAGE) Cr neutrino source measurement*, *Phys. Rev. Lett.* **77** (1996) 4708.
- [7] SAGE collaboration, *Measurement of the response of the Russian-American gallium experiment to neutrinos from a Cr-51 source*, *Phys. Rev.* **C59** (1999) 2246 [[hep-ph/9803418](#)].
- [8] J. Abdurashitov et al., *Measurement of the response of a Ga solar neutrino experiment to neutrinos from an Ar-37 source*, *Phys. Rev.* **C73** (2006) 045805 [[nucl-ex/0512041](#)].
- [9] GALLEX collaboration, *First results from the Cr-51 neutrino source experiment with the GALLEX detector*, *Phys. Lett.* **B342** (1995) 440.
- [10] GALLEX collaboration, *Final results of the Cr-51 neutrino source experiments in GALLEX*, *Phys. Lett.* **B420** (1998) 114.
- [11] F. Kaether, W. Hampel, G. Heusser, J. Kiko and T. Kirsten, *Reanalysis of the GALLEX solar neutrino flux and source experiments*, *Phys. Lett.* **B685** (2010) 47 [[1001.2731](#)].
- [12] MINOS+ collaboration, *Search for sterile neutrinos in MINOS and MINOS+ using a two-detector fit*, *Phys. Rev. Lett.* **122** (2019) 091803 [[1710.06488](#)].
- [13] NOVA collaboration, *Search for active-sterile neutrino mixing using neutral-current interactions in NOvA*, *Phys. Rev.* **D96** (2017) 072006 [[1706.04592](#)].
- [14] ICECUBE collaboration, *Searches for Sterile Neutrinos with the IceCube Detector*, *Phys. Rev. Lett.* **117** (2016) 071801 [[1605.01990](#)].
- [15] P. Machado, O. Palamara and D. Schmitz, *The Short-Baseline Neutrino Program at Fermilab*, *Ann. Rev. Nucl. Part. Sci.* **69** (2019) [[1903.04608](#)].
- [16] J. Park, *Searching for a Sterile Neutrino at J-PARC MLF: JSNS² experiment*, *PoS EPS-HEP2017* (2017) 128.
- [17] J. Hamann, S. Hannestad, G. Raffelt and Y. Wong, *Sterile neutrinos with eV masses in cosmology: How disfavoured exactly?*, *JCAP* **1109** (2011) 034 [[1108.4136](#)].

- [18] S. Hannestad, I. Tamborra and T. Tram, *Thermalisation of light sterile neutrinos in the early universe*, *JCAP* **1207** (2012) 025 [1204.5861].
- [19] S. Gariazzo, P. F. de Salas and S. Pastor, *Thermalisation of sterile neutrinos in the early Universe in the 3+1 scheme with full mixing matrix*, *JCAP* **1907** (2019) 014 [1905.11290].
- [20] S. Hagstotz, P. F. de Salas, S. Gariazzo, M. Gerbino, M. Lattanzi, S. Vagnozzi et al., *Bounds on light sterile neutrino mass and mixing from cosmology and laboratory searches*, 2003.02289.
- [21] K. Abazajian, N. Bell, G. Fuller and Y. Wong, *Cosmological lepton asymmetry, primordial nucleosynthesis, and sterile neutrinos*, *Phys. Rev.* **D72** (2005) 063004 [astro-ph/0410175].
- [22] A. Mirizzi, N. Saviano, G. Miele and P. Serpico, *Light sterile neutrino production in the early universe with dynamical neutrino asymmetries*, *Phys. Rev.* **D86** (2012) 053009 [1206.1046].
- [23] N. Saviano, A. Mirizzi, O. Pisanti, P. Serpico, G. Mangano and G. Miele, *Multi-momentum and multi-flavour active-sterile neutrino oscillations in the early universe: role of neutrino asymmetries and effects on nucleosynthesis*, *Phys. Rev.* **D87** (2013) 073006 [1302.1200].
- [24] S. Hannestad, R. Hansen and T. Tram, *How Self-Interactions can Reconcile Sterile Neutrinos with Cosmology*, *Phys. Rev. Lett.* **112** (2014) 031802 [1310.5926].
- [25] N. Saviano, O. Pisanti, G. Mangano and A. Mirizzi, *Unveiling secret interactions among sterile neutrinos with big-bang nucleosynthesis*, *Phys. Rev.* **D90** (2014) 113009 [1409.1680].
- [26] M. Archidiacono, S. Hannestad, R. Hansen and T. Tram, *Cosmology with self-interacting sterile neutrinos and dark matter - A pseudoscalar model*, *Phys. Rev.* **D91** (2015) 065021 [1404.5915].
- [27] M. Archidiacono, S. Gariazzo, C. Giunti, S. Hannestad, R. Hansen, M. Laveder et al., *Pseudoscalarsterile neutrino interactions: reconciling the cosmos with neutrino oscillations*, *JCAP* **1608** (2016) 067 [1606.07673].
- [28] X. Chu, B. Dasgupta and J. Kopp, *Sterile neutrinos with secret interactionslasting friendship with cosmology*, *JCAP* **1510** (2015) 011 [1505.02795].
- [29] X. Chu, B. Dasgupta, M. Dentler, J. Kopp and N. Saviano, *Sterile neutrinos with secret interactionscosmological discord?*, *JCAP* **1811** (2018) 049 [1806.10629].
- [30] G. Gelmini, S. Palomares-Ruiz and S. Pascoli, *Low reheating temperature and the visible sterile neutrino*, *Phys. Rev. Lett.* **93** (2004) 081302 [astro-ph/0403323].
- [31] G. Gelmini, E. Osoba, S. Palomares-Ruiz and S. Pascoli, *MeV sterile neutrinos in low reheating temperature cosmological scenarios*, *JCAP* **0810** (2008) 029 [0803.2735].
- [32] G. Gelmini, P. Lu and V. Takhistov, *Visible Sterile Neutrinos as the Earliest Relic Probes of Cosmology*, 1909.04168.
- [33] G. Gelmini, P. Lu and V. Takhistov, *Cosmological Dependence of Non-resonantly Produced Sterile Neutrinos*, 1909.13328.
- [34] C. Yaguna, *Sterile neutrino production in models with low reheating temperatures*, *JHEP* **06** (2007) 002 [0706.0178].
- [35] K. Abazajian, *Sterile neutrinos in cosmology*, *Phys. Rept.* **711-712** (2017) 1 [1705.01837].

- [36] P. de Salas, M. Lattanzi, G. Mangano, G. Miele, S. Pastor and O. Pisanti, *Bounds on very low reheating scenarios after Planck*, *Phys. Rev.* **D92** (2015) 123534 [1511.00672].
- [37] T. Hasegawa, N. Hiroshima, K. Kohri, R. Hansen, T. Tram and S. Hannestad, *MeV-scale reheating temperature and thermalization of oscillating neutrinos by radiative and hadronic decays of massive particles*, *JCAP* **12** (2019) 012 [1908.10189].
- [38] N. Bell, R. Volkas and Y. Wong, *Relic neutrino asymmetry evolution from first principles*, *Phys. Rev.* **D59** (1999) 113001 [hep-ph/9809363].
- [39] T. Venumadhav, F. Cyr-Racine, K. Abazajian and C. Hirata, *Sterile neutrino dark matter: Weak interactions in the strong coupling epoch*, *Phys. Rev.* **D94** (2016) 043515 [1507.06655].
- [40] S. Dodelson and L. Widrow, *Sterile-neutrinos as dark matter*, *Phys. Rev. Lett.* **72** (1994) 17 [hep-ph/9303287].
- [41] PARTICLE DATA GROUP collaboration, *Review of Particle Physics*, *Phys. Rev.* **D98** (2018) 030001.
- [42] E. Akhmedov, *Do non-relativistic neutrinos oscillate?*, *JHEP* **07** (2017) 070 [1703.08169].
- [43] B. McKellar and M. Thomson, *Oscillating doublet neutrinos in the early universe*, *Phys. Rev.* **D49** (1994) 2710.
- [44] G. Sigl and G. Raffelt, *General kinetic description of relativistic mixed neutrinos*, *Nucl. Phys.* **B406** (1993) 423.
- [45] X. Shi and G. Fuller, *A New dark matter candidate: Nonthermal sterile neutrinos*, *Phys. Rev. Lett.* **82** (1999) 2832 [astro-ph/9810076].
- [46] S. Hannestad, R. Hansen and T. Tram, *Can active-sterile neutrino oscillations lead to chaotic behavior of the cosmological lepton asymmetry?*, *JCAP* **1304** (2013) 032 [1302.7279].
- [47] PLANCK collaboration, *Planck 2018 results. VI. Cosmological parameters*, 1807.06209.
- [48] S. Hannestad, R. Hansen, T. Tram and Y. Wong, *Active-sterile neutrino oscillations in the early Universe with full collision terms*, *JCAP* **1508** (2015) 019 [1506.05266].
- [49] X. S. Li, *An overview of superlu: Algorithms, implementation, and user interface*, *ACM Trans. Math. Softw.* **31** (2005) 302.
- [50] J. W. Demmel, J. R. Gilbert and X. S. Li, *An asynchronous parallel supernodal algorithm for sparse gaussian elimination*, *SIAM J. Matrix Anal. Appl.* **20** (1999) 915.
- [51] M. Dentler, A. Hernandez-Cabezudo, J. Kopp, P. Machado, M. Maltoni, I. Martinez-Soler et al., *Updated Global Analysis of Neutrino Oscillations in the Presence of eV-Scale Sterile Neutrinos*, *JHEP* **08** (2018) 010 [1803.10661].
- [52] K. Kainulainen, *Light Singlet Neutrinos and the Primordial Nucleosynthesis*, *Phys. Lett.* **B244** (1990) 191.
- [53] M. Kawasaki, K. Kohri and N. Sugiyama, *Cosmological constraints on late time entropy production*, *Phys. Rev. Lett.* **82** (1999) 4168 [astro-ph/9811437].
- [54] M. Kawasaki, K. Kohri and N. Sugiyama, *MeV scale reheating temperature and thermalization of neutrino background*, *Phys. Rev.* **D62** (2000) 023506 [astro-ph/0002127].

- [55] E. Aver, K. Olive and E. Skillman, *The effects of He I $\lambda 10830$ on helium abundance determinations*, *JCAP* **1507** (2015) 011 [1503.08146].
- [56] Y. Izotov, T. Thuan and N. Guseva, *A new determination of the primordial He abundance using the He I $\lambda 10830$ emission line: cosmological implications*, *Mon. Not. Roy. Astron. Soc.* **445** (2014) 778 [1408.6953].
- [57] E. Zavarygin, J. Webb, S. Riemer-Sørensen and V. Dumont, *Primordial deuterium abundance at $z_{\text{abs}} = 2:504$ towards Q1009+2956*, *J. Phys. Conf. Ser.* **1038** (2018) 012012 [1801.04704].
- [58] R. J. Cooke, M. Pettini and C. C. Steidel, *One Percent Determination of the Primordial Deuterium Abundance*, *Astrophys. J.* **855** (2018) 102 [1710.11129].
- [59] L. Kawano, *Let's go: Early universe. 2. Primordial nucleosynthesis: The Computer way*, .
- [60] P. J. Kernan and L. M. Krauss, *Refined big bang nucleosynthesis constraints on Omega (baryon) and N (neutrino)*, *Phys. Rev. Lett.* **72** (1994) 3309 [astro-ph/9402010].
- [61] C. Angulo et al., *A compilation of charged-particle induced thermonuclear reaction rates*, *Nucl. Phys. A* **656** (1999) 3.
- [62] P. D. Serpico, S. Esposito, F. Iocco, G. Mangano, G. Miele and O. Pisanti, *Nuclear reaction network for primordial nucleosynthesis: A Detailed analysis of rates, uncertainties and light nuclei yields*, *JCAP* **12** (2004) 010 [astro-ph/0408076].
- [63] O. Pisanti, A. Cirillo, S. Esposito, F. Iocco, G. Mangano, G. Miele et al., *PARthENoPE: Public Algorithm Evaluating the Nucleosynthesis of Primordial Elements*, *Comput. Phys. Commun.* **178** (2008) 956 [0705.0290].
- [64] R. H. Cyburt and B. Davids, *Evaluation of Modern He-3(alpha,gamma)Be-7 Data*, *Phys. Rev. C* **78** (2008) 064614 [0809.3240].
- [65] M. Kawasaki, K. Kohri, T. Moroi and Y. Takaesu, *Revisiting Big-Bang Nucleosynthesis Constraints on Long-Lived Decaying Particles*, *Phys. Rev.* **D97** (2018) 023502 [1709.01211].
- [66] S. Hannestad, *What is the lowest possible reheating temperature?*, *Phys. Rev.* **D70** (2004) 043506 [astro-ph/0403291].
- [67] M. Reno and D. Seckel, *Primordial Nucleosynthesis: The Effects of Injecting Hadrons*, *Phys. Rev.* **D37** (1988) 3441.
- [68] K. Kohri, *Primordial nucleosynthesis and hadronic decay of a massive particle with a relatively short lifetime*, *Phys. Rev.* **D64** (2001) 043515 [astro-ph/0103411].
- [69] M. Kawasaki, K. Kohri and T. Moroi, *Big-Bang nucleosynthesis and hadronic decay of long-lived massive particles*, *Phys. Rev.* **D71** (2005) 083502 [astro-ph/0408426].
- [70] T. Sjostrand, S. Mrenna and P. Z. Skands, *PYTHIA 6.4 Physics and Manual*, *JHEP* **05** (2006) 026 [hep-ph/0603175].
- [71] T. Sjostrand, S. Mrenna and P. Z. Skands, *A Brief Introduction to PYTHIA 8.1*, *Comput. Phys. Commun.* **178** (2008) 852 [0710.3820].

- [72] DAYA BAY collaboration, *Improved Search for a Light Sterile Neutrino with the Full Configuration of the Daya Bay Experiment*, *Phys. Rev. Lett.* **117** (2016) 151802 [1607.01174].
- [73] Y. Declais et al., *Search for neutrino oscillations at 15-meters, 40-meters, and 95-meters from a nuclear power reactor at Bugey*, *Nucl. Phys.* **B434** (1995) 503.
- [74] PROSPECT collaboration, *First search for short-baseline neutrino oscillations at HFIR with PROSPECT*, *Phys. Rev. Lett.* **121** (2018) 251802 [1806.02784].
- [75] F. Megas, *eV-scale Sterile Neutrino Investigation with the First Tritium KATRIN Data*, Ph.D. thesis, MSc Thesis, Munich University, 2019.
- [76] PTOLEMY collaboration, *Neutrino physics with the PTOLEMY project: active neutrino properties and the light sterile case*, *JCAP* **1907** (2019) 047 [1902.05508].
- [77] S. Gariazzo, C. Giunti, M. Laveder and Y. F. Li, *Updated Global 3+1 Analysis of Short-BaseLine Neutrino Oscillations*, *JHEP* **06** (2017) 135 [1703.00860].
- [78] S. Gariazzo, C. Giunti, M. Laveder, Y. F. Li and E. M. Zavanin, *Light sterile neutrinos*, *J. Phys.* **G43** (2016) 033001 [1507.08204].